Computational Study of an Axisymmetric Dual Throat Fluidic Thrust Vectoring Nozzle for a Supersonic Aircraft Application

Karen A. Deere*, Jeffrey D. Flamm†, Bobby L. Berrier‡, and Stuart K. Johnson§
NASA Langley Research Center, Hampton, VA, 23681-0001

A computational investigation of an axisymmetric Dual Throat Nozzle concept has been conducted. This fluidic thrust-vectoring nozzle was designed with a recessed cavity to enhance the throat shifting technique for improved thrust vectoring. The structured-grid, unsteady Reynolds-Averaged Navier-Stokes flow solver PAB3D was used to guide the nozzle design and analyze performance. Nozzle design variables included extent of circumferential injection, cavity divergence angle, cavity length, and cavity convergence angle. Internal nozzle performance (wind-off conditions) and thrust vector angles were computed for several configurations over a range of nozzle pressure ratios from 1.89 to 10, with the fluidic injection flow rate equal to zero and up to 4 percent of the primary flow rate. The effect of a variable expansion ratio on nozzle performance over a range of freestream Mach numbers up to 2 was investigated. Results indicated that a 60° circumferential injection was a good compromise between large thrust vector angles and efficient internal nozzle performance. A cavity divergence angle greater than 10° was detrimental to thrust vector angle. Shortening the cavity length improved internal nozzle performance with a small penalty to thrust vector angle. Contrary to expectations, a variable expansion ratio did not improve thrust efficiency at the flight conditions investigated.

Nomenclature

A_1 = primary nozzle throat area, 4.6 in^2
A_2 = primary nozzle exit area, in^2
A_2/A_1 = expansion ratio
A_s = secondary fluidic injection plenum minimum area, $A_s = w \cdot r_1 d\beta$, in^2
$C_{d,prim}$ = discharge coefficient of primary nozzle, $(w_p + w_s) / w_{i,p}$
$C_{f,g\ sys}$ = system thrust ratio, $F_R / (F_{i,p} + F_{i,s})$
CD = convergent-divergent
CFD = computational fluid dynamics
config = configuration
DTN = dual throat nozzle
d_1 = diameter at upstream minimum area, in
d_2 = diameter at nozzle exit, in
$d\beta$ = circumferential injection angle, radians
F_A = axial force, lb
$F_{i,p}$ = ideal isentropic thrust of primary nozzle, lb
$F_{i,s}$ = ideal isentropic thrust of secondary fluidic injection flow, lb
F_N = normal force, lb
F_R = resultant force, $\sqrt{F_A^2 + F_N^2 + F_S^2}$, lb
F_S = side force, lb
JETF = Jet Exit Test Facility
k = turbulent kinetic energy per unit mass, ft^2/s^2

* Aerospace Engineer, Configuration Aerodynamics Branch, MS 499, AIAA Senior Member.
† Aerospace Engineer, Configuration Aerodynamics Branch, MS 499, AIAA Associate Fellow.
‡ Distinguished Research Associate, Configuration Aerodynamics Branch, MS 499, AIAA Fellow.
§ Aerospace Engineer, Advanced Aerospace Systems Branch, MS 411.

l = length of primary nozzle cavity, in (fig. 4)
l_1 = length from upstream minimum area to cavity apex, in (fig. 4)
l_2 = length from cavity apex to nozzle exit, in (fig. 4)
M_∞ = freestream Mach number
NPR = nozzle pressure ratio, $p_{t,j} / p_\infty$
NPR_D = design nozzle pressure ratio
p = surface static pressure, psi
$p_{t,j}$ = total pressure of primary flow, psi
$p_{t,s}$ = total pressure of secondary fluidic injection flow, psi
p_∞ = freestream static pressure, psi
r_1 = radius at upstream minimum area, in
SVC = Shock-Vector Control
TS = Throat Shifting
VER = Variable Expansion Ratio
w = width of the injection slot, in
$w_{i,p}$ = ideal primary weight flow, lb/sec
$w_{i,s}$ = ideal secondary fluidic injection weight flow, lb/sec
w_p = actual primary weight flow, lb/sec
w_s = actual secondary fluidic injection weight flow, lb/sec
x, y, z = Cartesian coordinates
y^+ = nondimensional first cell height
δ_p = pitch thrust-vector angle, $\tan^{-1}(F_N / F_A)$
δ_y = yaw thrust-vector angle, $\tan^{-1}(F_S / F_A)$
ε = dissipation rate of turbulent kinetic energy, ft^2/s^3
η = thrust-vectoring efficiency, $\delta_p /[w_s / (w_s + w_p) * 100]$, deg/%-injection
ϕ = secondary flow injection angle, 150 deg (fig. 4)
θ_1 = cavity divergence angle, deg
θ_2 = cavity convergence angle, deg

I. Introduction

Thrust vectoring is a candidate technology for a supersonic aircraft that may help satisfy take-off and landing requirements and offer additional design options for lower sonic-boom configurations. Proper tailoring of the airplane lift distribution is one factor in lower airplane sonic-boom signatures. Utilization of thrust vectoring nozzles with a canard airframe configuration may allow more optimal tailoring of the lift distribution during cruise for lower sonic-boom signatures than possible with conventional configurations. Additionally, thrust vectoring could augment conventional controls for some control power to trim the aircraft and thus reduce cruise trim drag. Thrust vectoring can be a valuable control effector at low dynamic pressures, where traditional aerodynamic control technologies are less effective. There are two fundamental methods to accomplish thrust vectoring, fluidic and mechanical. Fluidic thrust vectoring systems offer the potential for structurally fixed nozzles, which have the potential for substantial weight reductions compared to mechanical thrust vectoring nozzles that require actuated hardware to force the exhaust flow off axis.

Fluidic thrust vectoring is the manipulation or control of the primary exhaust flow with the use of a secondary air source, which is typically bleed air from the engine compressor or fan. There are three primary mechanisms of fluidic thrust vectoring: shock-vector control, throat shifting, and counterflow[1-13]. These techniques can be used to vector the exhaust flow in the pitch and yaw directions. All thrust vectoring techniques are evaluated with some common parameters; nozzle discharge coefficient, system thrust ratio, thrust vector angle and thrust vectoring efficiency. Thrust vectoring efficiency η is an important parameter to evaluate and compare the ability of different configurations to vector the primary exhaust flow with a given amount of secondary fluidic injection.

The shock-vector control (SVC) method[1-8] uses supersonic flow turning through shocks created by fluidic injection in the divergent section of a convergent-divergent (CD) nozzle. Working best at off-design, over-expanded flow conditions, large thrust vector angles are generated with SVC techniques at the expense of system thrust ratio as the flow is robustly turned, and flow losses occur, through shocks in the nozzle. Throat shifting (TS) methods[8-11] more efficiently manipulate the subsonic flow upstream of the throat. This technique shifts and skews the nozzle throat plane by fluidic injection at the nozzle throat and typically achieve higher system thrust ratios than shock-vector control methods, but usually generate smaller thrust vector angles. Unlike the two previously described

thrust-vectoring techniques, the counterflow method uses suction in a slot between a primary CD nozzle and an aft collar[12-13]. The counterflow technique can produce large thrust vector angles with little secondary suction flow requirements, but issues such as suction supply source, hysteresis effects, and airframe integration need to be addressed.

The technique of interest in this paper is a throat shifting method enhanced with separation control. The current technique has been researched at NASA LaRC both computationally and experimentally[14-17] and is denoted as the Dual Throat Nozzle (DTN) concept because of the two minimum areas that form a convergent-divergent-convergent nozzle shape. Large thrust vector angles are generated with fluidic injection at the upstream minimum area, which controls separation and maximizes pressure differentials in the recessed cavity created between the two throats as indicated in figure 1. Figure 2 shows a comparison of experimental results on a two-dimensional (2D) rectangular DTN and computational results on an axisymmetric DTN, with several other TS and SVC thrust vectoring nozzle concepts that are documented in references 2-9 and 16. Results indicate that the DTN technique achieves larger thrust vectoring efficiencies than the other fluidic thrust vectoring techniques. Additionally, DTN has the highest system thrust ratio than all the other methods for NPR<8. Only one SVC technique has a better system thrust ratio than the DTN for NPR=10 because the design NPR for that SVC nozzle is NPR_D=14.6 and the DTN is much farther off design.

The objective of the current work was to use the computational flow solver PAB3D to guide the design of an axisymmetric Dual Throat Nozzle and to evaluate the axisymmetric DTN with a variable expansion ratio capability. PAB3D was used to guide the design of the original 2D DTN[14] and results were verified experimentally[16] in the Jet Exit Test Facility (JETF) at the NASA LaRC. Several computational fluid dynamics (CFD) design and experimental validation cycles were completed on the 2D DTN and results indicated that PAB3D accurately predicted performance trends[15, 17]. Therefore, PAB3D was used with some confidence to guide the design of an axisymmetric version of the Dual Throat Nozzle concept with the results documented herein. The experimental evaluation of the axisymmetric DTN is documented in a companion paper[18].

II. Nozzle Design

A. Dual Throat Nozzle Design

A sketch of the Dual Throat Nozzle (DTN) concept is shown in Figure 1. The DTN geometry is intended to enhance the thrust vectoring capability of the throat shifting method by manipulating flow separation in a recessed cavity. The recessed cavity section is located between upstream and downstream minimum areas and fluidic injection is introduced at the upstream minimum area location. In a flight vehicle, pitch thrust vectoring could be implemented with top or bottom injection plenums (figure 3(a)), while yaw thrust vectoring, if needed as a control effector, would be implemented with right or left injection plenums (figure 3(b)). For the computational investigation, pitch thrust vectoring was simulated with a slot at the upstream minimum area, along the bottom of the nozzle. The experimental test implemented pitch thrust vectoring through a row of holes at the upstream minimum area along the bottom of the nozzle.

The geometry definitions for the DTN configurations are listed in Table 1. The upstream and downstream minimum areas are fixed at A_1=4.6 in^2. Figure 4 presents the geometric design variables that were investigated in this computational study; cavity divergence angle (θ_1), cavity convergence angle (θ_2), and cavity length (l). The effects of circumferential injection on thrust vectoring and internal nozzle performance was evaluated and a sketch is shown in figure 5. The configurations exploring these variables were simulated with a static freestream Mach number at nozzle pressure ratios from 1.89 to 10 and with secondary fluidic injection from 0- to 4-percent of the primary flow rate. Additionally, the effects of freestream Mach number on internal nozzle performance were investigated.

The extent of circumferential injection was investigated at 45°, 60°, and 90° for the full nozzle configurations. However, due to the symmetry of the flow, the full nozzle was modeled with a half plane mesh to save computational resources. Therefore, the half plane computational mesh had circumferential injection of 22.5°, 30° and 45°, respectively. Further meshing details will follow in the Computational Method section. The minimum area of the injection slot, A_s=0.066 in^2, was chosen to maintain choked flow in the injection slot for a 3% secondary injection flow rate at all NPR. Therefore, the injection width of each plenum was determined from the equation for A_s and the results are listed in Table 2. Every nozzle had an injection angle rotated 150° from the primary flow direction (figure 4).

Throughout the text, configuration 202 with 60° circumferential injection and an injection minimum slot width of 0.0525 inches for choked flow at a 3% injection rate will be referred to as the baseline nozzle.

Configuration	θ_1, °	θ_2, °	l_1, *in.*	l_2, *in.*	d_2, *in.*	l, in.	A_2/A_1	NPR_D
102	15	30	3.593	1.667	2.420	5.26	1	1.89
202	10	30	4.040	1.220	2.420	5.26	1	1.89
302	10	30	3.225	0.985	2.420	4.21	1	1.89
402	10	20	2.836	1.374	2.420	4.21	1	1.89

Table 1. DTN geometry definitions.

Full Geometry Circumferential Injection	Half-plane Computational Circumferential Injection	r_1, in.	$d\beta$, *radians*	w, in.
45°	22.5°	1.21	0.7854	0.0700
60°	30°	1.21	1.0472	0.0525
90°	60°	1.21	1.5708	0.0350

Table 2. Geometry descriptions for three circumferential injections.

B. Nozzle Design for the DTN with Variable Expansion Ratio Capability

It was of interest to modify the DTN configuration for supersonic applications. Therefore, nozzle performance needed to be optimized for flight Mach numbers and NPR ranges from take-off and landing (approximately M_∞=0.2 with NPR=1.89) to cruise (approximately M_∞=2 with NPR=10). Typically, a variable expansion ratio nozzle would be used over such a broad range of conditions to optimize thrust performance. However, once the exit area (expansion ratio) is increased to meet higher NPR and Mach number requirements, the Dual Throat Nozzle concept becomes a convergent-divergent nozzle with a small recessed cavity and thrust vectoring nozzle performance is compromised. However, large thrust vector angles would not be required at high-speed (cruise) conditions. In application, the aircraft designer would be selective about the nozzle designs to either get the most thrust vectoring with some penalties in thrust efficiency (e.g. at low speed) or to maintain thrust efficiency while compromising on small units of thrust vectoring (e.g. at high speed). Data will be presented for the Dual Throat Nozzle concept (A_2/A_1=1) and for a DTN with variable expansion ratio capability where expansion ratio is matched to the flight conditions, such that the potential tradeoffs between thrust vectoring and nozzle thrust performance can be better understood.

Increasing expansion ratio is simulated with a hinge at the cavity apex, which is located at the maximum diameter of the cavity. Opening up the convergent flaps at the hinge point reduces θ_2, increases exit area, and increases expansion ratio. Increasing exit area changes the DTN to an approximation of a convergent-divergent nozzle with a single geometric minimum, at what was previously denoted as the upstream throat location, while simultaneously reducing the nozzle cavity depth.

The DTN with a variable expansion ratio capability was designed by decreasing θ_2 from the angle for the DTN configuration (A_2/A_1=1) to a θ_2 angle optimum for M_∞=2 (A_2/A_1=1.97), with several design points in between. Cavity length was thought to be a critical parameter and was held constant during variations of θ_2 to document the impacts of θ_2 only, on internal nozzle performance. Therefore, the cavity convergent flap length decreased as θ_2 decreased for increasing expansion ratio and nozzle pressure ratio. This is not typical of variable geometry convergent-divergent nozzles, which have a hinge mechanism at the minimum area. For variable convergent-divergent nozzles, the flap flow path length remains constant with variations in expansion ratio. In an application of a DTN with variable expansion ratio capability, there would be a hinge at the cavity apex. Hence, increasing cavity expansion ratio with increasing NPR would actually cause the cavity length to increase, but the flow path length along the cavity convergent flap would remain constant.

The current work documents a first attempt to investigate a DTN with a variable expansion ratio. The geometry definitions for the variable expansion ratio configurations are shown in Table 3. The diameter at the upstream minimum area is constant at d_1=2.42 inches for all nozzles and therefore, the primary upstream minimum area is fixed at A_1=4.6 in^2. There are three DTNs with a variable expansion ratio capability that are discussed in the Results section and they are denoted as VER 200, VER 300, and VER 400. The VER 200 nozzle has the geometry definition of configuration 202 at NPR=1.89, the geometry definition of 206 at NPR=6, and the geometry definition of 210 at NPR=10. Likewise, the VER 300 nozzle has the geometry definition of configuration 302 at NPR=1.89, the geometry definition of 306 at NPR=6, and the geometry definition of 310 at NPR=10. Finally, VER 400 has the geometry definition of configuration 402 at NPR=1.89, the geometry definition of 406 at NPR=6, and the geometry definition of 410 at NPR=10.

All the configurations were simulated with a static freestream Mach number at nozzle pressure ratios from 1.89 to 10 and with secondary fluidic injection from 0- to 4-percent of the primary flow rate. Additionally, the effects of freestream Mach number on internal nozzle performance were investigated.

Configuration	θ_1, °	θ_2, °	l_1, *in.*	l_2, *in.*	d_2, *in.*	l, in.	A_2/A_1	NPR_D	M_∞
102	15	30	3.593	1.667	2.420	5.26	1	1.89	0.1
202	10	30	4.040	1.220	2.420	5.26	1	1.89	0.2
203	10	28	4.040	1.220	2.53	5.26	1.09	3	0.6
204	10	25	4.040	1.220	2.672	5.26	1.22	4	0.9
205	10	22.7	4.040	1.220	2.806	5.26	1.34	5	1.2
206	10	20	4.040	1.220	2.940	5.26	1.47	6	1.4
208	10	15.4	4.040	1.220	3.156	5.26	1.70	8	1.7
210	10	11	4.040	1.220	3.360	5.26	1.92	10	2.0
302	10	30	3.225	0.985	2.420	4.21	1	1.89	0.1
306	10	17.4	3.225	0.985	2.940	4.21	1.47	6	0.1
310	10	5.72	3.225	0.985	3.360	4.21	1.92	10	0.1
402	10	20	2.836	1.374	2.420	4.21	1	1.89	0.1
406	10	9.91	2.836	1.374	2.940	4.21	1.47	6	0.1
410	10	1.25	2.836	1.374	3.360	4.21	1.92	10	0.1

Table 3. Geometry definitions for all configurations investigated.

III. Computational Method

The CFD code PAB3D was used to predict internal nozzle performance and freestream flow effects for the axisymmetric, fluidic thrust vectoring, DTN concept and the DTN with a variable expansion capability. PAB3D was chosen for this work because it was originally developed as an internal flow, propulsion code and now has been well tested and documented for predicting complex flow features in aeropropulsive, as well as aerodynamic configurations[19-26]. Additionally, PAB3D successfully predicted internal nozzle performance trends of the 2D rectangular DTN[15]. Extensive details of PAB3D are found in references 19 through 34 and code documentation is located at http://www.asm-usa.com/software/PAB3D/PAB3D-Doc.html. Pressure distributions, nozzle performance and thrust vector angles were computed with the PAB3D post processor code, POST. The POST software package documentation is located at http://www.asm-usa.com/software/PAB3D/doc/post/.

For the current work, the unsteady Reynolds-averaged Navier-Stokes equations were solved with a linear k-ε turbulence model. The van Leer flux vector-splitting scheme[35], the Roe flux difference-splitting scheme and the Spekereijse-Venkate limiter were all implemented in each block. A modified Jones and Launder form of the damping function[36] was implemented in the wall-bounded blocks to treat the singularity at the wall and a high Reynolds number model was selected for the freestream blocks. Solutions are third-order accurate in space. A dual time sub-iteration scheme[33] was used for the time advancement formulation to achieve second-order accuracy in time.

PAB3D requires a structured-mesh computational domain and a multiblock[20] feature allows the domain to be partitioned into sections, which is critical for modeling complex configurations like the DTN and for efficiently running the parallel version of PAB3D. Due to the symmetry of the flow, the three-dimensional axisymmetric nozzle configurations were modeled with half the nozzle. The computational mesh along the nozzle symmetry plane is shown in figure 6(a). Therefore, the computational mesh for the injection slot and plenum (figure 6(b)) were half of the full circumferential injections of 45°, 60°, and 90° shown in figure 5. To avoid having a collapsed pole of grid cells at the center of the nozzle, a C-grid along the nozzle walls was wrapped around an H-grid in the core of the nozzle (figure 6(c)). The C-grid spacing in the circumferential direction was 1.25 deg/cell, which matched 1:1 with the core H-grid. The baseline configuration (configuration 202) had 40 internal nozzle blocks, 1 injection plenum block, and 30 external freestream domain blocks. The far field boundaries were located 4 cavity lengths downstream and 2 cavity lengths upstream of the nozzle exit. The radial far field boundary was located 5 cavity lengths around the nozzle. The first grid height in the boundary layer was defined for y^+=0.5 on the fine mesh spacing for adequate modeling of the boundary layer flow and its interaction with secondary flow injection.

Several boundary conditions were used for this study. Riemann invariants along the characteristics were implemented along the lateral and in-flow freestream boundaries. At the downstream far field boundary, a subsonic, constant pressure outflow boundary condition was used, which automatically switches to first order extrapolation if

the flow is supersonic. The primary nozzle flow and the fluidic injection flow were specified with a fixed total-temperature and total-pressure boundary condition. A no-slip, adiabatic wall boundary condition was implemented on nozzle surfaces to obtain viscous solutions. For the current axisymmetric nozzle configuration, half the nozzle was modeled but a full configuration was simulated with a symmetry boundary condition.

The experimental data was recorded in the Jet Exit Test Facility at static conditions with no external freestream flow, but PAB3D will not tolerate a M_∞=0 freestream flow. Therefore, the computations with 'static freestream conditions' required a small external freestream flow (M_∞=0.1) for computational stability.

IV. Results

A. DTN Unvectored: Effects of Cavity Divergence Angle on Internal Nozzle Performance

The effects of cavity divergence angle (θ_1) on internal nozzle performance were studied with the 2D DTN concept[16]. Results indicated that θ_1>10° caused flow separation from the upper and lower cavity divergent flaps in the 2D DTN, at all flow conditions. Additionally, introducing fluidic injection did not cause flow attachment on the opposite cavity wall for θ_1>10°. Therefore, two cavity divergence angles (10° and 15°) were investigated with the axisymmetric DTN concept to verify previous 2D results with the axisymmetric geometry.

Discharge coefficient and thrust ratio for the axisymmetric DTN (A_2/A_1=1) with θ_1=15° and θ_1=10° are shown in Table 4 for several NPR with no fluidic injection. For the θ_1=10° configuration, discharge coefficient is over 4% higher and thrust ratio is over 1% higher than the θ_1=15° configuration for all NPR. The effects of cavity divergence angle on static pressure distributions along the nozzle surfaces are shown in figure 7 for several NPR with no fluidic injection. The relatively flat pressure ratio distribution between x=0 in. and x=3 in. for θ_1=15° (configuration 102) indicates separated flow from the cavity divergent flap. The increasing pressure ratios for 0<x<3 in. for θ_1=10° (configuration 202) indicates continuous flow expansion along the nozzle divergent flap. Discharge coefficient of the θ_1=15° configuration is lower than the θ_1=10° configuration because the separated flow in θ_1=15° cavity decreases the effective minimum area compared to the attached flow in the θ_1=10° cavity.

Figure 8 shows the total pressure contours in the nozzle for θ_1=15° and θ_1=10° at NPR=1.89. Separated flow is identified with a loss in total pressure. A total pressure loss is present with configuration 102 (θ_1=15°), with the primary core flow about 5 psi higher than most of the flow in the cavity apex. The flow is not separated for configuration 202 (θ_1=10°) and the total pressure is nearly constant throughout the nozzle. Since the DTN concept in thrust vectoring mode works substantially better when the flow is not separated from the divergent nozzle wall during unvectored flow (no injection) mode, θ_1=10° was selected for subsequent configurations.

Configuration	θ_1	M_∞	*NPR*	$C_{d,prim}$	$C_{f,g\ sys}$	w_p, *lb/sec*
102	15°	0.1	1.89	0.845	0.946	2.5
102	15°	0.1	6	0.886	0.950	8.3
102	15°	0.1	10	0.885	0.925	13.9
202	10°	0.1	1.89	0.893	0.994	2.6
202	10°	0.1	6	0.933	0.966	8.7
202	10°	0.1	10	0.929	0.937	14.5

Table 4. Effect of cavity divergence angle on nozzle performance at several NPR with no fluidic injection.

B. DTN Unvectored: Internal Nozzle Performance

Figure 9 presents the internal nozzle performance for three axisymmetric DTNs (A_2/A_1=1). The only difference in nozzle performance between the three DTN configurations occurs in discharge coefficient for NPR_D=1.89. Figure 10 presents the Mach contours for the three DTN configurations at NPR=1.89 with no fluidic injection. Configuration 402 has the short cavity length, the smallest cavity convergence angle and the highest discharge coefficient at NPR=1.89. Configuration 402 has a larger region of supersonic flow at the upstream throat and the flow is not decelerated as much in the cavity apex region as configuration 202 and 302.

As expected, system thrust ratio drops with increasing NPR for all three DTN configurations because they are designed for NPR_D=1.89. The flow becomes underexpanded with increasing NPR beyond 1.89 and some thrust is lost in the expansion of the flow in the plume, external to the nozzle. Therefore, the performance penalty with increasing NPR might preclude the use of the DTN unless thrust vectoring was an overriding mission requirement of the aircraft.

C. DTN: Effects of Circumferential Injection on Thrust Vectoring and Internal Nozzle Performance

Configuration 202 was used to determine the effects of slot circumferential injection on thrust vectoring and internal nozzle performance. Figure 5 presents the three circumferential injections investigated and data at NPR=1.89 with a nominal 3% injection is shown in Table 5. Results indicate that substantial thrust vector angles and thrust vectoring efficiencies are achieved with all circumferential injections at the nominal takeoff and landing NPR. The 90° circumferential injection produced the largest thrust vector angle because it produces the most separation in the cavity. The 45° circumferential injection had the best discharge coefficient and system thrust ratio because the smaller circumferential injection causes the least amount of flow separation in the cavity. Therefore, the 60° circumferential injection was chosen for all the thrust vectoring simulations as a reasonable compromise between thrust vector angle, discharge coefficient, and system thrust ratio.

Full Geometry Circumferential Injection	*%–injection*	$C_{d,prim}$	$C_{f,g\ sys}$	δ_p, °	η, °/%
45°	2.97	0.761	0.945	15.61	5.25
60°	2.97	0.756	0.937	16.32	5.50
90°	2.95	0.75	0.930	16.68	5.65

Table 5. Effect of circumferential injection on nozzle performance for Configuration 202, A_2/A_1=1, NPR=1.89, 3% injection.

D. DTN: Baseline Thrust Vectoring and Internal Nozzle Performance

The effect of injection rate on internal nozzle performance and thrust vectoring for the baseline nozzle at NPR=1.89 is shown in Table 6. Reasonable thrust vector angles are achieved with very little fluidic injection flow. A fluidic injection rate as low as 0.125% of the primary flow rate generated a thrust vectoring efficiency of 59.8°/%-injection with a good system thrust ratio for a fluidic injection nozzle. Thrust vector angle increases with percent injection, although the thrust vectoring efficiency is much higher at the lower injection rates. Large penalties in discharge coefficient and modest losses in system thrust ratio occur as injection rate increases. Increasing secondary injection flow rate decreases the effective minimum area in the nozzle, which substantially decreases discharge coefficient. Total pressure losses due to shocks and separated flow in the recessed cavity cause losses in system thrust ratio.

%-Injection	$C_{d,prim}$	$C_{f,g\ sys}$	δ_p, °	η, °/%	$p_{t,s}$, psi	*Choked Secondary Flow*
0.125	0.940	0.969	7.47	59.8	23	no
0.5	0.828	0.966	9.26	19.1	25.2	no
1	0.812	0.960	11.4	11.3	27.3	no
2	0.781	0.947	14.09	7.0	32.5	no
3	0.756	0.937	16.32	5.5	43	yes
4	0.735	0.925	17.56	4.4	56.7	yes

Table 6. Effects of injection rate for the baseline nozzle (configuration 202), w=0.0525 inches, NPR=1.89.

The baseline nozzle (configuration 202 with a 60° circumferential injection) was designed to operate at NPR=1.89 with 3% injection. The effect of lower injection flow rates were investigated using the baseline nozzle even though the flow in the secondary plenum was not choked at injection rates less than 3% (Table 6). When it was discovered that large thrust vector angles were achieved with low injection rates, it became of interest to understand the impact of a choked injection flow at those low injection rates. Thus, configuration 202 was modified with an injection slot minimum width of 0.0175 inches and data was computed at injection rates of 1%, 2%, and 3% of the primary flow rate (Table 7). A choked fluidic injection flow improved thrust vector angles 1.25°-1.8° as the supersonic fluidic injection flow penetrated further into the primary nozzle flow than the unchoked subsonic injection flow, but had a negative impact on discharge coefficient and system thrust ratio. As the secondary injection flow penetrated further into the primary nozzle flow, effective minimum area was restricted and discharge coefficient dropped.

%-Injection	$C_{d,prim}$	$C_{f,g\ sys}$	δ_p, °	η, °/%	$p_{t,s}$, psi	*Choked Secondary Flow*
1	0.792	0.950	13.14	13.21	47	yes
2	0.762	0.937	15.89	7.85	91.3	yes
3	0.743	0.929	17.55	5.90	131	yes

Table 7. Effects of injection rate for modified Configuration 202, w=0.0175 inches, NPR=1.89.

The effects of nozzle pressure ratio on thrust vectoring and internal nozzle performance, and on Mach contours of the baseline DTN with 3% injection are shown in figures 11 and 12, respectively. The discharge coefficient is flat and the nozzle flow is choked with the sonic line skewed at the nozzle exit for NPR>2. At NPR=1.89, the flow is mostly subsonic and the primary nozzle is not choked. The sonic line and internal nozzle flow are remarkably similar for NPR>2, which accounts for the flat nature of $C_{d,prim}$.

System thrust ratios are over 0.935 for the range of NPR with 3% injection, which is good for a fluidic thrust vectoring nozzle (figure 2). Thrust ratio is lowest at NPR=1.89 when the nozzle is not choked, and peaks at NPR=4 when the sonic line is fixed at the nozzle exit. As NPR increases, thrust ratio slightly decreases as the flow in the DTN is underexpanded and thrust is lost in the expansion of the flow in the plume.

Thrust vector angle decreases with increasing NPR, with the biggest drop between NPR=1.89 and NPR=4. Increasing the jet total pressure from 27.8 psi (NPR=1.89) to 58.8 psi (NPR=4) chokes the primary flow with a sonic line at the nozzle exit. The secondary flow penetrates and asymmetrically restricts part of the primary exhaust flow. This asymmetric restriction encourages separated flow along a portion of the circumference of the cavity and attached flow along most of the remaining cavity walls. Axial slices of Mach contours through the cavity (not shown) indicate similar flow separation for both NPR=1.89 and NPR=4. The primary differences between these two solutions are more expansion at the upstream throat and a sonic line at the downstream throat for the NPR=4 solution. These results indicate that the fixed sonic line that occurs for NPR>1.89 with 3% injection dampens the thrust vectoring capability compared to the design NPR. However, the DTN still generates substantial thrust vector angles over 10° for NPR up to 10.

E. DTN: Effects of Cavity Length and Cavity Convergence Angle on Thrust Vectoring and Nozzle Performance

The effects of cavity length on nozzle performance and thrust vectoring were investigated to determine if a shorter cavity nozzle, for reduced propulsion weight, could generate the same levels of thrust efficiency and thrust vectoring efficiency as the baseline DTN. Also, the effects of cavity convergence angle were investigated with the shorter cavity (l=4.2 inches).

The effects of cavity length and convergence angle on discharge coefficient, system thrust ratio and thrust vectoring efficiency for three DTN (A_2/A_1=1) configurations over the NPR range with 3% fluidic injection are shown in figure 13. Shortening the cavity length from 5.26 inches to 4.21 inches (compare configurations 202 and 302) has a beneficial effect on discharge coefficient, little effect on system thrust ratio, and a detrimental impact on thrust vectoring efficiency. For the shorter cavity length, decreasing cavity convergence angle from 30° to 20° (compare configurations 302 and 402) improves discharge coefficient, slightly decreases system thrust ratio, and reduces thrust vectoring efficiency.

Figure 14 presents the Mach contours for configurations 202, 302 and 402 at NPR=1.89 with a 3% injection flow rate. As the nozzle is shortened (represented by the change from 202 to 302) and then cavity convergence angle is decreased (represented by the change from 302 to 402), the region of higher Mach number flow (green contours) in the cavity apex gets thicker and the region of separated flow gets smaller. These flow contours indicate an increased region of effective area, that may cause the increase in discharge coefficient with decreasing cavity length and convergence angle (figure 13(a)). Also, as this region of high Mach number flow increases, it appears to decrease the thrust vector angle of the primary flow, as indicated with the black arrows in figure 14. This follows the trend of decreasing thrust vector efficiency as the cavity length and convergence angle decreases in figure 13(c).

F. DTN Variable Expansion Ratio: Unvectored Flow Results

A variable expansion ratio capability was added to DTN (A_2/A_1=1) configurations 202, 302 and 402. Geometry definitions are listed in Table 3. Figures 15 and 16 present unvectored, internal nozzle performance for the DTN with variable expansion ratio capability for A_2/A_1=1, 1.47 and 1.92. The dashed line in each figure represents a DTN with variable expansion ratio (VER) capability that would have A_2/A_1=1 for NPR_D=1.89, a larger expansion ratio of A_2/A_1=1.47 for NPR_D=6 and the maximum expansion ratio of A_2/A_1=1.92 for NPR_D=10.

The system thrust ratio results appear to contradict the hypothesis that a variable expansion ratio capability would be more thrust efficient than the DTN operating over the range of NPR. However, a closer inspection of the data at NPR=6 indicates some hope of achieving a more efficient variable expansion ratio capability with design optimization of the A_2/A_1=1.47 setting. The VER 200 has the worst performance at NPR_D=6, but system thrust ratio improves by decreasing cavity length and cavity convergence angle to the VER 400 configuration. The total pressure contours in figure 17 help to describe the flow characteristics of the nozzles that impact system thrust ratio.

The DTNs with variable expansion ratio capability at the A_2/A_1=1.47 setting (NPR_D=6) have a normal shock inside the nozzle that substantially decreases system thrust ratio. The flow instantaneously goes from supersonic to

subsonic flow, which results in a huge total pressure loss that is illustrated in figures 17(b), 17(e) and 17(h). The large total pressure drop inside configurations 206, 306, and 406 decreases system thrust ratio to much lower values than the DTN (A_2/A_1=1) configurations 202, 302, and 402 operating at NPR=6 (figure 15). As the expansion ratio increases to the A_2/A_1=1.92 (NPR_D=10) setting, the flow remains supersonic inside the nozzle and the flow adjusts the higher jet total pressure to the lower ambient pressure through oblique shocks that culminate outside the nozzle (figures 17(c), 17(f) and 17(i)). The normal shock is outside the nozzle for the long cavity (figure 17(c)), but is completely eliminated for the nozzles with the short cavity (figures 17(f) and 17(i)). As the normal shock is eliminated, figure 15(d) shows increases in system thrust ratio for the short cavity nozzles compared to the long cavity nozzle at NPR=10. Certainly, data in figure 15 at the supersonic cruise NPR_D=10 condition indicates an improvement in thrust ratio with the variable expansion ratio compared to the fixed DTN operating at NPR=10. Moreover, data in figure 15(c) indicates that thrust ratio may be greater than 0.966 over the range of NPR by using A_2/A_1=1 (configuration 402) for NPR<5 and A_2/A_1=1.92 (configuration 410) for NPR≥5. With this combination of expansion ratios, thrust efficiency at take-off, landing and supersonic cruise would be greater than 0.986. Additionally, configuration 402 generates good thrust vector angles at take-off and landing conditions (NPR=1.89), with a thrust vectoring efficiency at 4.2°/%-injection (figure 13).

The discharge coefficients shown in figure 16 for each DTN (A_2/A_1=1) are significantly lower than the DTNs with variable expansion ratio capability. The DTN has two equal minimum areas, while the rest of the nozzles have one minimum area at the upstream injection location. The DTN has a sonic line at the nozzle exit for NPR>2, which decreases effective minimum area because the cavity flow is subsonic, turbulent, and has a slightly lower total pressure that results in a thicker boundary layer at the exit. However, configurations with A_2/A_1>1 have a fixed sonic line at the upstream minimum area and a much thinner boundary layer that allows more weight flow to pass through the nozzle for constant and higher discharge coefficients that the DTN.

G. DTN Variable Expansion Ratio: Thrust Vectoring Results

The effects of a variable expansion ratio on thrust vectoring and internal nozzle performance, and on Mach contours are shown in figures 18 and 19, respectively. All solutions are computed with a 3% injection flow rate and with a static freestream flow M_∞=0.1. The data in figure 18 includes configurations 202 (A_2/A_1=1 DTN) at NPR=1.89, 204 (A_2/A_1=1.22) at NPR=4, 206 (A_2/A_1=1.47) at NPR=6, 208 (A_2/A_1=1.7) at NPR=8 and 210 (A_2/A_1=1.92) at NPR=10. All configurations have a cavity length of 5.21 inches. Geometry descriptions of each configuration are found in Table 3.

Increasing expansion ratio with increasing NPR improves discharge coefficient 6-12% at NPR>4.0 during thrust vectoring operation, compared to operating the DTN over the range of NPR, compare figures 11(a) and 18(a). The curvature in discharge coefficient for the DTN with variable expansion ratio capability is indicative of flow that is changing in the nozzle. There is no sonic line at NPR=1.89 and the sonic lines that are present in the Mach contours (figure 19) for NPR=4 and NPR=8 are different. At NPR>6, the sonic line becomes fixed and discharge coefficient flattens out.

The hypothesis for using a DTN with variable expansion ratio capability is to improve nozzle performance over a range of NPR. Surprisingly, large improvements in system thrust ratio did not result from using a variable expansion ratio during thrust vectoring operation (compare figure 11(b) and figure 18(b)). For A_2/A_1>1, the cavity flow becomes supersonic and filled with strong shocks that decrease thrust compared to the mostly subsonic flow in the DTN (A_2/A_1=1) cavity. In fact, when comparing all plots in figures 11 and 18, it appears that using the DTN over the flight envelope is the best compromise of nozzle thrust vectoring performance, with higher system thrust ratios over the entire range and larger thrust vector angles for NPR>5. Even though a DTN with variable expansion ratio capability has higher discharge coefficients over the range of NPR than the DTN configuration, a constant discharge coefficient would be more favorable than one that changes with flight conditions. The DTN configuration could be oversized to compensate for the low discharge coefficient and provide the proper mass flow for the engine.

Thrust vector angle for the DTN with variable expansion ratio capability drops off quickly for NPR>4 and A_2/A_1=1.22. As the nozzle changes from a DTN configuration to an approximate convergent-divergent shaped nozzle with increasing A_2/A_1, the cavity flow becomes supersonic (figure 19) and harder to influence with the constant level of 3% fluidic injection. However, large thrust vector angles are most important at take-off and landing conditions and a thrust vector angle over 16° was generated at those conditions.

H. Effects of Freestream Mach number

Since the experimental investigation in the Jet Exit Test Facility was done with no external freestream flow, most of the computational simulations investigating the DTN were computed with a near static freestream external flow (M_∞=0.1). However, it is of great interest to also investigate the effects of an external flow on internal nozzle performance and thrust vectoring of the DTN concept. It should be noted that no attempt has been made to optimize the nozzle boattail closure. Thus, external drag was not quantitatively evaluated in the current study.

The effects of freestream Mach number on the internal nozzle performance for the DTN and for the DTN with variable expansion ratio capability are shown in figures 20 and 21, respectively. From these data, it appears that the freestream flow has little or no impact on discharge coefficient, system thrust ratio or thrust vector angle.

Figure 22 presents the comparison of Mach contours for the DTN at a NPR=10 with 3% injection for a M_∞=0.1 freestream flow and a M_∞=2 freestream flow. As previously discussed, the sonic line remains at the nozzle exit for all NPR>2 and there is no influence of the M_∞=0.1 or the M_∞=2 freestream flow on nozzle internal exhaust flow. Thus, nozzle internal performance and thrust vectoring performance for the two extremes of freestream Mach number flow are nearly identical, figure 20. At NPR=1.89 (M_∞=0.2 condition), the flow is completely subsonic through the nozzle and no sonic line exists at the nozzle exit. However, the velocity of the freestream external flow at M_∞=0.2 is less than the velocity of the internal nozzle exhaust flow, and thus, there is no influence of the freestream flow on internal performance or thrust vectoring for the NPR=1.89 case, either.

Figure 23 presents the comparison of Mach contours for the expansion ratio A_2/A_1=1.92 nozzle at a NPR=10 with 3% injection for a M_∞=0.1 freestream flow and a M_∞=2 freestream flow. Almost all of the internal nozzle flow is supersonic and downstream disturbances (such as external flow effects) cannot feed upstream into the nozzle. Thus, internal nozzle performance and thrust vectoring performance for the M_∞=0.1 and M_∞=2 freestream flows are almost identical, figure 21.

The separated flow along the boattail may decrease the sensitivity of the freestream flow impacts on the internal nozzle flow. It should be apparent from a comparison of Mach contours for the M_∞=2.0 supersonic cruise in figures 22 and 23 that the DTN will have a much larger boattail separation problem than the DTN with variable expansion ratio set at A_2/A_1=1.92. This is because the nozzle boattail angle and aft projected area are both decreased as the aft convergent flap is opened up (θ_2 decreased) to increase nozzle exit diameter and expansion ratio. This would indicate that the DTN with variable expansion ratio capability would have a propulsion integration benefit over the DTN that was not evaluated in the current paper.

V. Conclusions

The design of an axisymmetric, fluidic thrust vectoring Dual Throat Nozzle was guided with the aid of the structured-grid, unsteady Reynolds-Averaged Navier-Stokes flow solver PAB3D. The nozzle design variables that were investigated include extent of circumferential injection, cavity divergence angle, cavity length, cavity convergence angle, and expansion ratio. Additionally, the effects of an external freestream flow on thrust vector angle and nozzle internal performance were investigated. Computational results that helped assess the axisymmetric DTN design and the affects of variable expansion ratio are summarized below.

1. Internal nozzle performance (unvectored with no injection) for the Dual Throat Nozzle and for the Dual Throat Nozzle with variable expansion ratio capability indicates that operating the Dual Throat Nozzle over the range of nozzle pressure ratio would be a better compromise for thrust efficiency than using a variable expansion ratio design that would require additional weight to the propulsion system. However, further design optimization of the mid-cruise configuration may increase system thrust ratio above Dual Throat Nozzle and thus, prove that the variable expansion ratio design is worthy of the additional weight to the propulsion system.
2. A 60° circumferential injection provides the best compromise between thrust vector angle and internal nozzle performance.
3. Similar to computational and experimental results on the two-dimensional Dual Throat Nozzle, a cavity divergence angle greater than 10° is detrimental to thrust vector angle. The flow completely separates from the axisymmetric Dual Throat Nozzle cavity walls instead of maintaining an asymmetric flow pattern that boosts pressure differential and thrust vector angle.
4. Choked secondary injection flow increases thrust vector angle as the supersonic injection flow penetrates further into the primary flow than unchoked subsonic injection flow, but negatively impacts discharge coefficient up to 2% and system thrust ratio up to 1%.

5. Shortening the nozzle, for decreased propulsion weight, improves discharge coefficient and system thrust ratio for a small penalty in thrust vector angle.
6. During thrust vectoring operation, the Dual Throat Nozzle provides a better compromise to thrust vector angle and internal nozzle performance than a Dual Throat Nozzle with variable expansion ratio capability over the range of NPR and Mach numbers researched.
7. External nozzle flow has little to no impact on thrust vector angle and internal nozzle performance over the range of NPR and Mach numbers researched. This is important since all experimental data to date on the DTN has been collected with a static freestream and this result indicates that little to no impact would be expected on internal nozzle flow and thrust vector angles during wind tunnel testing at wind-on freestream conditions. However, boattail closure was not optimized and separated flow along the boattail may decrease the sensitivity of the impacts of freestream flow on internal nozzle flow.

References

[1]Anderson, C. J.; Giuliano, V. J.; and Wing, David J.: Investigation of Hybrid Fluidic / Mechanical Thrust Vectoring for Fixed-Exit Exhaust Nozzles. AIAA 97-3148, July 1997.

[2]Abeyounis, W. K.; and Bennett, B. D. Jr.: Static Internal Performance of an Overexpanded, Fixed-Geometry, Nonaxisymmetric Nozzle with Fluidic Pitch-Thrust-Vectoring Capability. NASA TP-3645, October 1997.

[3]Chiarelli, C.; Johnsen, R. K.; Shieh, C. F.; Wing, D. J.: Fluidic Scale Model Multi-Plane Thrust Vector Control Test Results. AIAA 93-2433, June 1993.

[4]Giuliano, V. J.; and Wing, David J.: Static Investigation of a Fixed-Aperture Exhaust Nozzle Employing Fluidic Injection for Multiaxis Thrust Vector Control. AIAA 97-3149, July 1997.

[5]Wing, David J.; and Giuliano, V. J.: Fluidic Thrust Vectoring of an Axisymmetric Exhaust Nozzle at Static Conditions. ASME FEDSM97-3228, June 1997.

[6]Deere, K. A.: Computational Investigation of the Aerodynamic Effects on Fluidic Thrust Vectoring. AIAA 2000-3598, July 2000.

[7]Waithe, Kenrick A.: An Experimental and Computational Investigation of Multiple Injection Ports in a Convergent-Divergent Nozzle for Fluidic Thrust Vectoring. Master of Science Thesis, May 2001.

[8]Deere, K. A.: Summary of Fluidic Thrust Vectoring Research Conducted at NASA Langley Research Center. AIAA-2003-3800, June 2003.

[9]Yagle, P. J., Miller, D. N., Ginn, K. B.; and Hamstra, J. W.: Demonstration of Fluidic Throat Skewing for Thrust Vectoring in Structurally Fixed Nozzles. 2000-GT-0013, May 8-11, 2000.

[10]Deere, Karen A.; and Wing, David J.: PAB3D Simulations of a Nozzle with Fluidic Injection for Yaw-Thrust-Vector Control. AIAA 98-3254, July 1998.

[11]Miller, D. N.; Yagle, P. J.; and Hamstra, J. W.: Fluidic Throat Skewing for Thrust Vectoring in Fixed Geometry Nozzles. AIAA 99-0365, January 1999.

[12]Hunter, C.A. and Deere, Karen A.: Computational Investigation of Fluidic Counterflow Thrust Vectoring. AIAA 99-2669, June 1999.

[13]Flamm, J. D.: Experimental Study of a Nozzle Using Fluidic Counterflow for Thrust Vectoring. AIAA 98-3255, July 1998.

[14]Deere, K. A.; Berrier, B. L.; Flamm, J. D.; and Johnson, S. K.: Computational Study of Fluidic Thrust Vectoring Using Separation Control in a Nozzle. AIAA-2003-3803, June 2003.

[15]Deere, K. A.; Berrier, B. L.; Flamm, J. D.; and Johnson, S. K.: A Computational Study of a New Dual Throat Fluidic Thrust Vectoring Nozzle Concept. AIAA-2005-3502, July 2005.

[16]Flamm, J. D.; Berrier, B. L.; Johnson, S. K.; and Deere, K. A.: An Experimental Study of a Dual Throat Fluidic Thrust Vectoring Nozzle Concept. AIAA-2005-3503, July 2005.

[17]Flamm, J. D.; Deere, K. A.; Berrier, B. L.; and Johnson, S. K.: Design Enhancements of the Two-Dimensional, Dual Throat Fluidic Thrust Vectoring Nozzle Concept. AIAA-2006-3701, June 2006.

[18]Flamm, J. D.; Deere, K. A.; Mason, M. L.; Berrier, B. L.; and Johnson, S. K.: Experimental Study of an Axisymmetric Dual Throat Fluidic Thrust Vectoring Nozzle for a Supersonic Aircraft Application. AIAA-2007-5084, July 2007.

[19]Abdol-Hamid, K. S.: The Application of 3D Marching Scheme for the Prediction of Supersonic Free Jets. AIAA 89-2897. July 1989.

[20]Abdol-Hamid, K. S.: Application of a Multiblock/ Multizone Code (PAB3D) for the Three-Dimensional Navier-Stokes Equations. AIAA-91-2155, June 1991.

[21]Carlson, J. R.: A Nozzle Internal Performance Prediction Method. NASA TP 3221, October 1992.

[22]Carlson, J. R.: Computational Prediction of Isolated Performance of an Axisymmetric Nozzle at Mach Number 0.90. NASA TM 4506, February 1994.

[23]Pao, S. P., Carlson, J. R., and Abdol-Hamid, K. S.: Computational Investigation of Circular-to-Rectangular Transition Ducts. Journal of Propulsion and Power, Vol. 10, No. 1, p 95-100, Jan.-Feb. 1994.

[24]Abdol-Hamid, K. S.; Lakshmanan, B.; and Carlson, J. R.: Application of Navier-Stokes Code PAB3D With k-ε Turbulence Model to Attached and Separated Flows. NASA TP-3480, January 1995.

[25]Abdol-Hamid, K. S., Carlson, J. R., and Pao, S. P.: Calculation of Turbulent Flows Using Mesh Sequencing and Conservative Patch Algorithm. AIAA 95-2336, July 1995.

[26]Pao, S. P.; and Abdol-Hamid, K. S.: Numerical Simulation of Jet Aerodynamics Using the Three-Dimensional Navier-Stokes Code PAB3D. NASA TP 3596, September 1996.
[27]Carlson, J. R.: Applications of Algebraic Reynolds Stress Turbulence Models Part 1: Incompressible Flat Plate. Journal of Propulsion and Power, Vol. 13, No. 5, p 610-619, Sept.-Oct. 1997.
[28]Abdol-Hamid, K., Pao, S., Massey, S., and Elmiligui, A.: Temperature Corrected Turbulence Model for High Temperature Jet Flow. ASME Journal of Fluids Engineering, Vol. 126, No. 5, September 2004.
[29]Balakrishnan, L.; and Abdol-Hamid, K. S.: A Comparative Study of Two Codes with an Improved Two-Equation Turbulence Model For Predicting Jet Plumes. AIAA 92-2604, June 1992.
[30]Girimaji, S. S.: Fully-Explicit and Self-Consistent Algebraic Reynolds Stress Model. Inst. For Computer Applications in Science and Engineering, 95-82, December 1995.
[31]Abdol-Hamid, K. S.: Implementation of Algebraic Stress Models in a General 3-D Navier-Stokes Method (PAB3D). NASA CR-4702, 1995.
[32]Abdol-Hamid, K. S. and Girimaji, S. S.: A Two-Stage Procedure Toward the Efficient Implementation of PANS and Other Hybrid Turbulence Models. NASA/TM-2004-213260, August 2004.
[33]Massey, S. J.; and Abdol-Hamid, K. S.: Enhancement and Validation of PAB3D for Unsteady Aerodynamics. AIAA 2003-1235, January 2003.
[34]Elmiligui, A., Abdol-Hamid, K., and Hunter, C.: Numerical Investigation of Flow in an Over-expanded Nozzle with Porous Surfaces. AIAA 2005-4159, July 2005.
[35]van Leer, B.: Flux-Vector Splitting for the Euler Equations. ICASE Report 82-30, 1982.
[36]Jones, W. P.; and Launder, B. E.: The Prediction of Laminarization With a Two-Equation Model of Turbulence. Int. Journal of Heat & Mass Transfer, vol. 15, no. 2, February 1972, pp. 301-314.

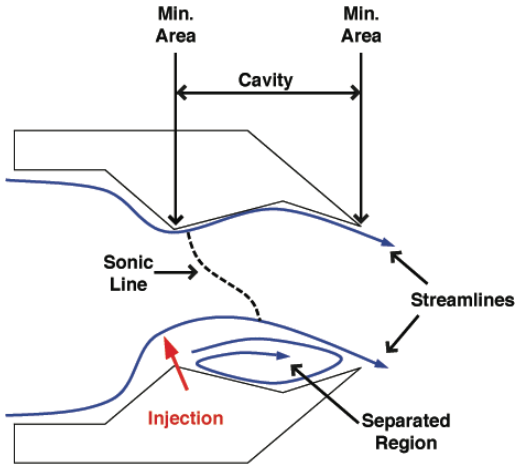

Figure 1. Sketch of the Dual Throat Nozzle with fluidic injection at the upstream minimum area.

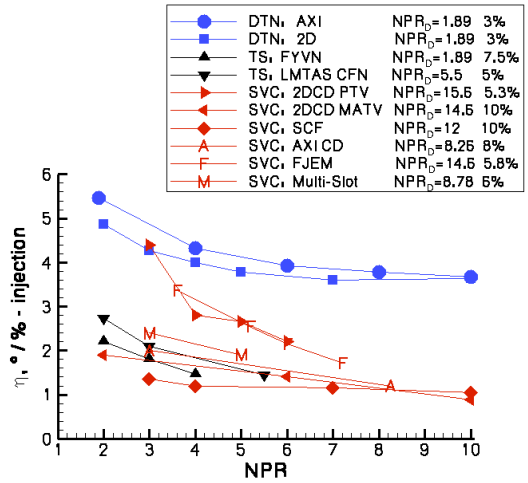

(a) Thrust Vectoring Efficiency

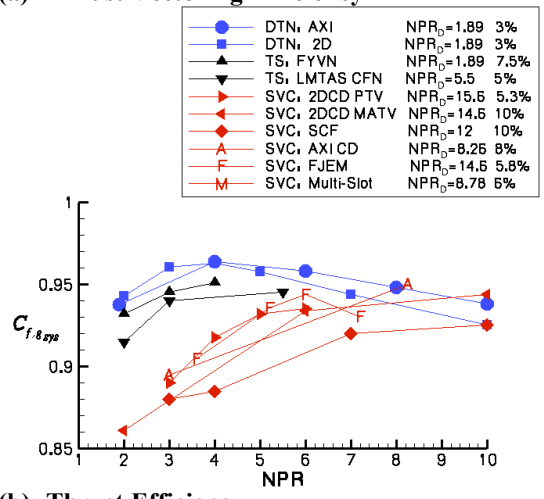

(b) Thrust Efficiency

Figure 2. Comparison of dual throat nozzle (DTN) thrust vectoring efficiency and thrust efficiency to other Throat Shifting (TS) and Shock-Vector Control (SVC) methods.

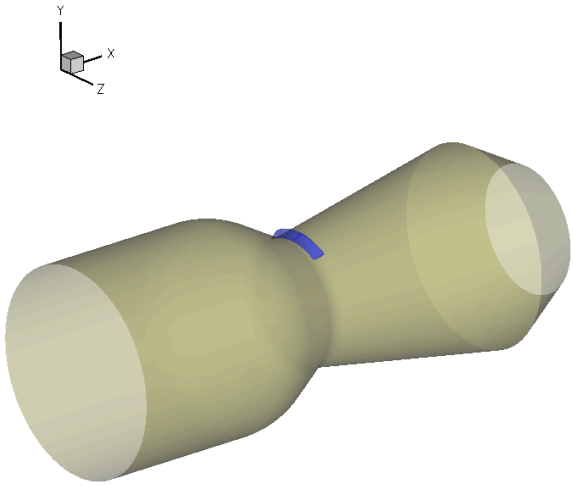

(a) Pitch injection plenum shown in blue.

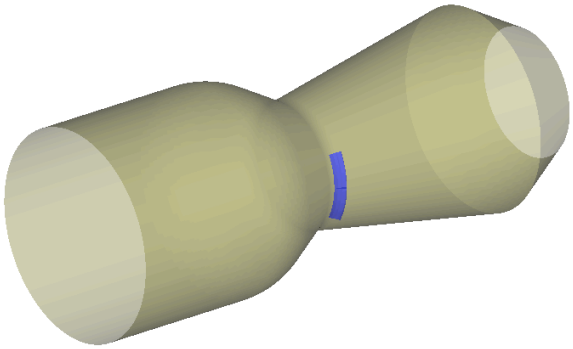

(b) Yaw injection plenum shown in blue.

Figure 3. Axisymmetric DTN with injection plenum located at the upstream minimum area.

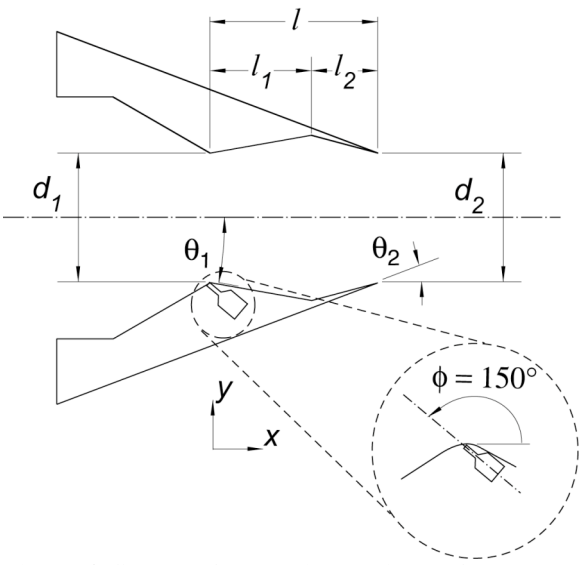

Figure 4. Sketch of the design variables for DTN.

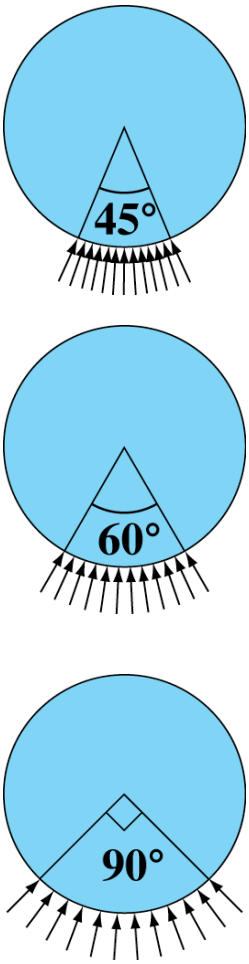

Figure 5. Extent of circumferential injection.

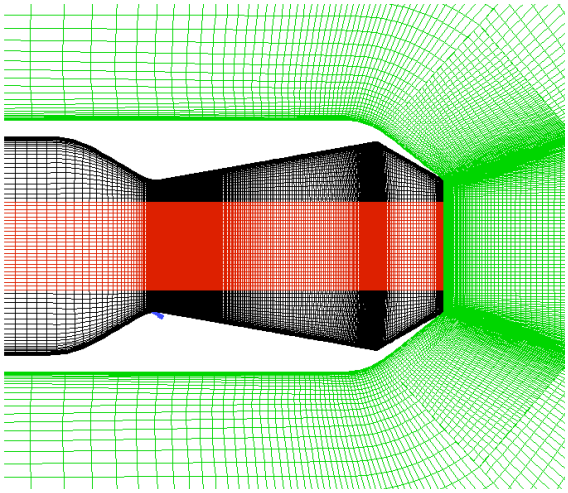

(a) Symmetry plane

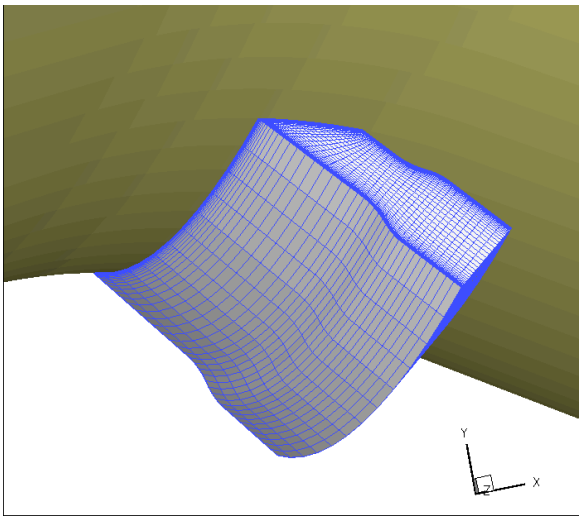

(b) Injection plenum

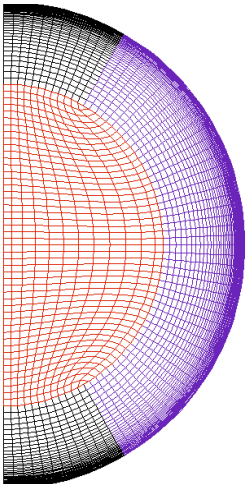

(c) C-grid wrapped around the core H-grid

Figure 6. Some views of the computational mesh.

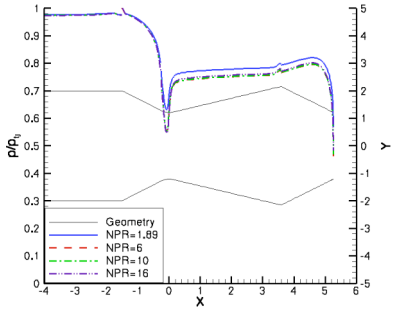

(a) Configuration 102, θ_I=15°

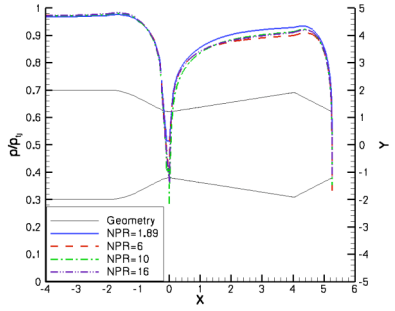

(b) Configuration 202, θ_I=10°

Figure 7. Pressure distributions for several NPR with no fluidic injection.

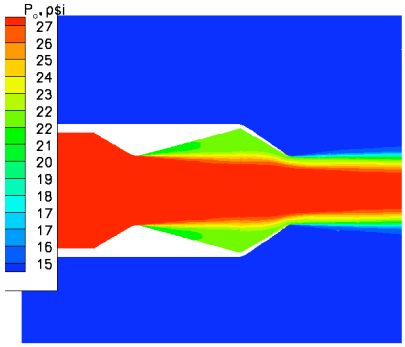

(a) **θ_I=15°, configuration 102**

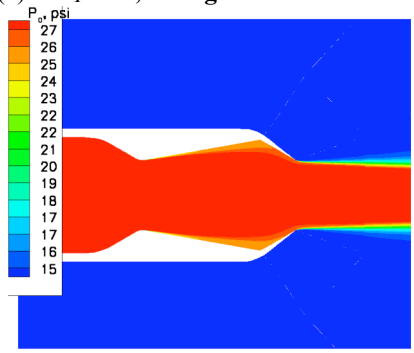

(b) θ_I=10°, configuration 202

Figure 8. Total Pressure contours for NPR=1.89 with no fluidic injection.

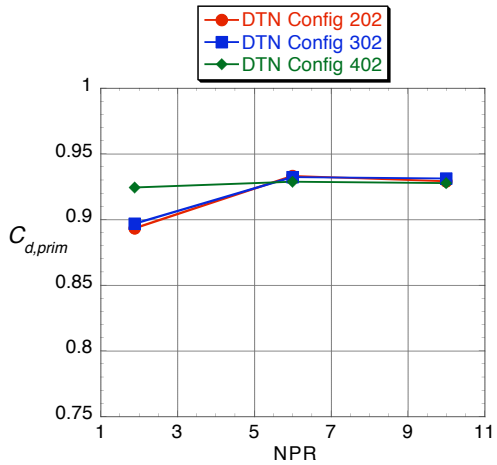

(a) Discharge coefficient

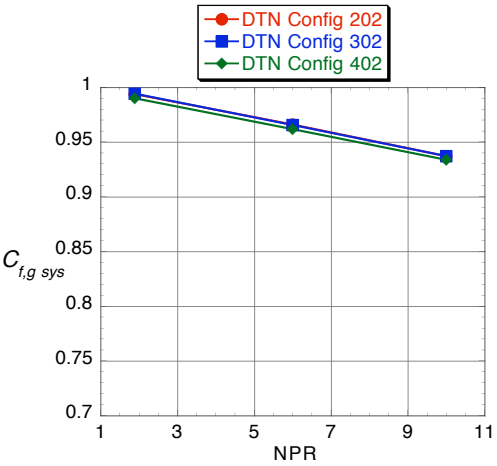

(b) System Thrust ratio

Figure 9. DTN no injection internal nozzle performance.

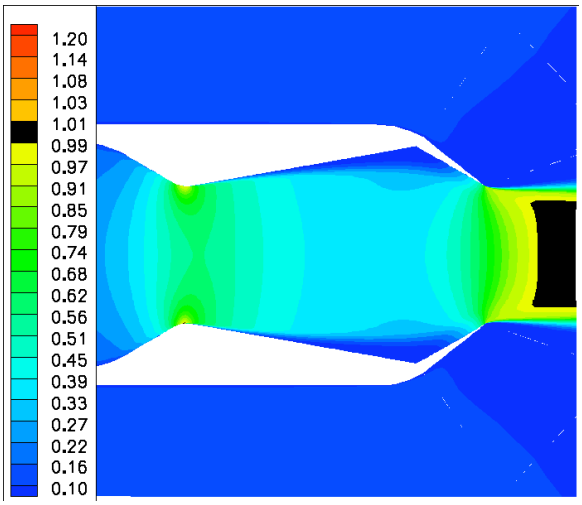

(a) Configuration 202

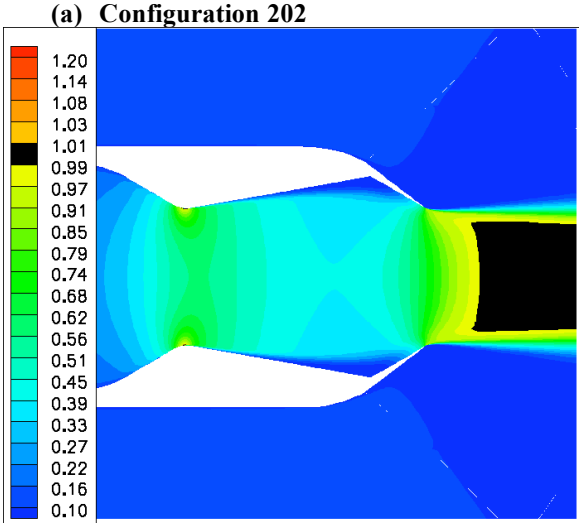

(b) Configuration 302

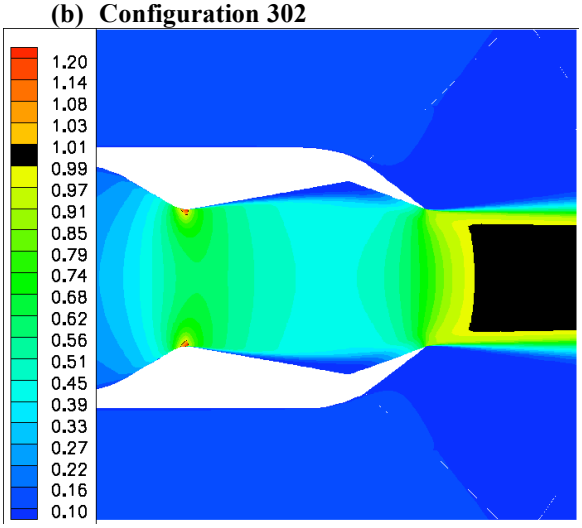

(c) Configuration 402

Figure 10. Mach contours for three DTNs at NPR=1.89, no injection.

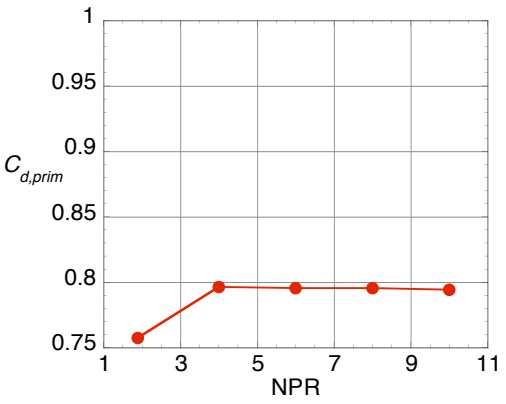

(a) Discharge coefficient

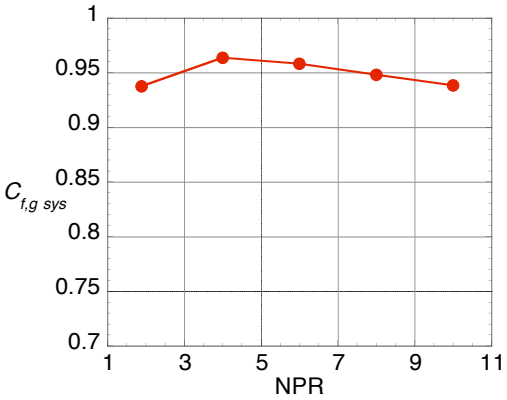

(b) System thrust ratio

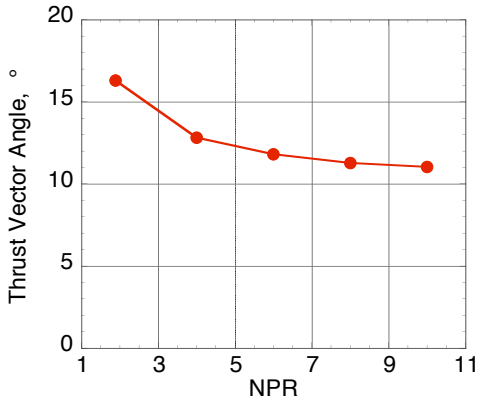

(c) Thrust vector angle

Figure 11. Effect NPR on thrust vectoring and internal nozzle performance for the DTN (configuration 202, A_2/A_1=1), 3% fluidic injection, M_∞=0.1.

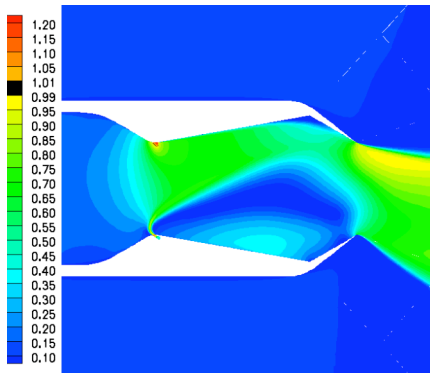

(a) NPR=1.89

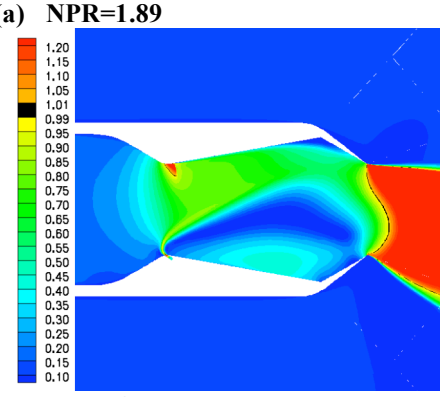

(b) NPR=4

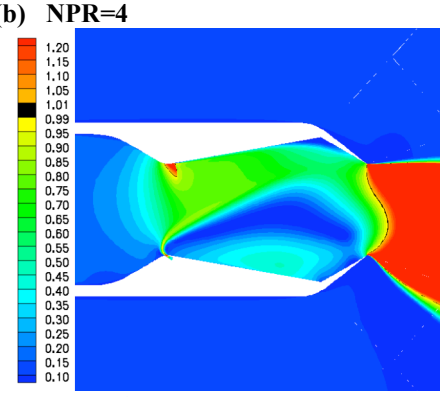

(c) NPR=6

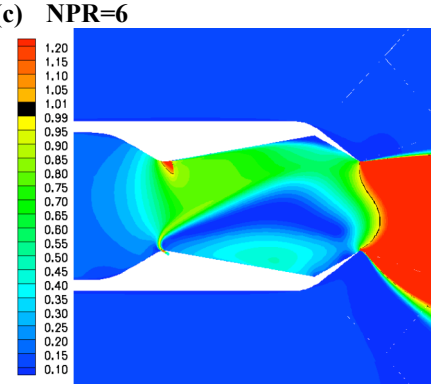

(d) NPR=8

Figure 12. Effect of NPR on Mach contours for the DTN (configuration 202, A_2/A_1=1), 3% fluidic injection, M_∞=0.1.

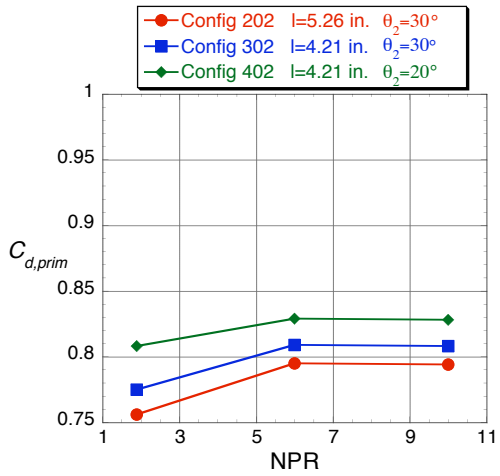

(a) Discharge Coefficient

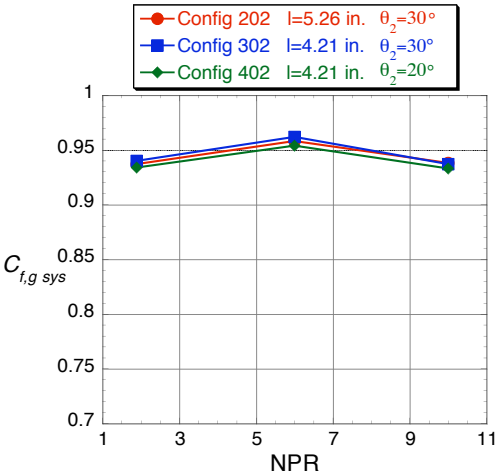

(b) System Thrust Ratio

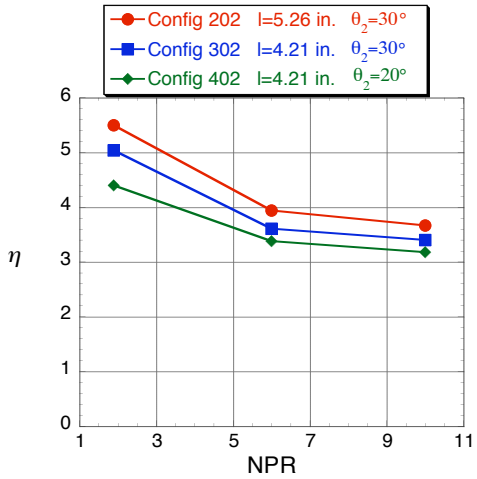

(c) Thrust vectoring efficiency

Figure 13. Effect of cavity length and convergence angle on nozzle performance of three DTNs (A_2/A_1=1) with 3% fluidic injection.

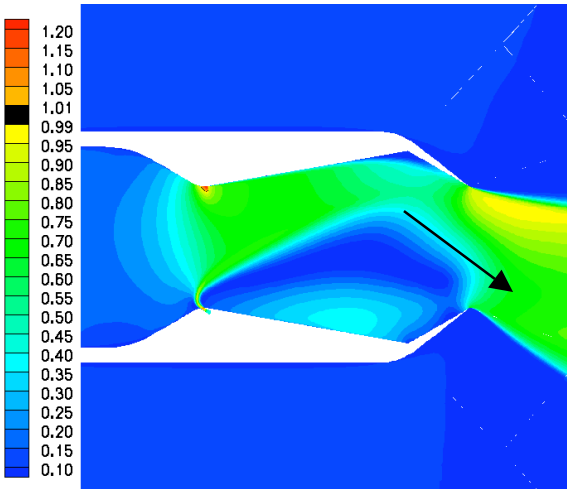

(a) Configuration 202, l=5.26 in., θ_2=30°

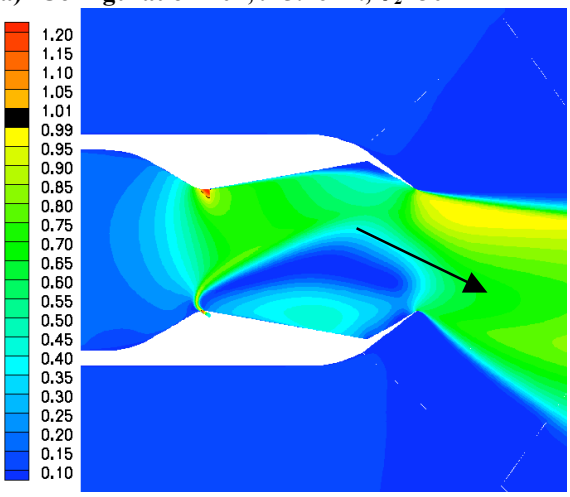

(b) Configuration 302, l=4.21 in., θ_2=30°

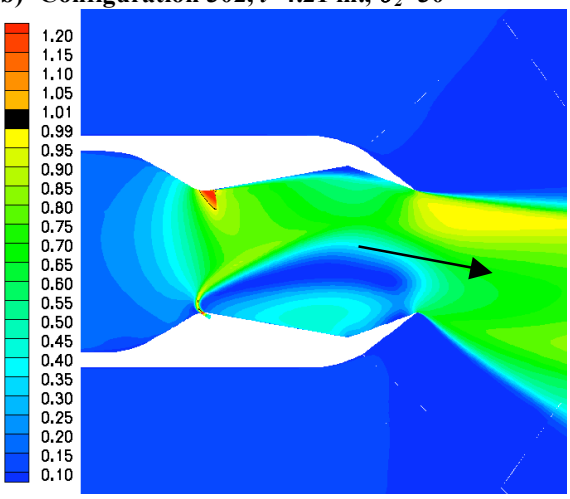

(c) Configuration 402, l=4.21 in., θ_2=20°

Figure 14. Effect of cavity length and cavity convergence angle on Mach contours of three DTNs (A_2/A_1=1), NPR=1.89, 3% fluidic injection.

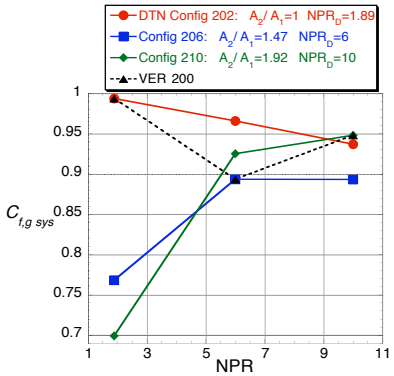

(a) l=5.26 in., l_1=4.04 in., l_2=1.22 in.

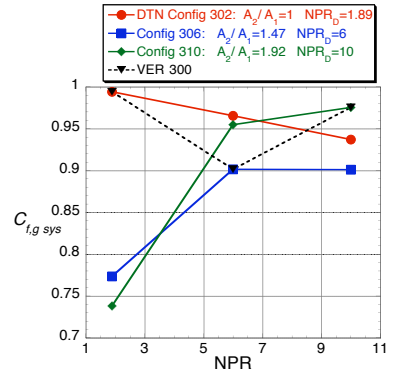

(b) l=4.21 in., l_1=3.225 in., l_2=0.985 in.

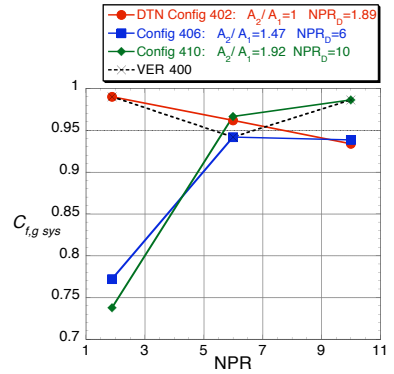

(c) l=4.21 in., l_1=2.836 in., l_2=1.374 in.

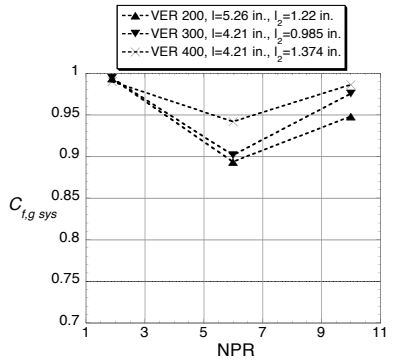

(d) Variable expansion ratio (VER) nozzles

Figure 15. Effect of a variable expansion ratio on unvectored (no injection) system thrust ratio.

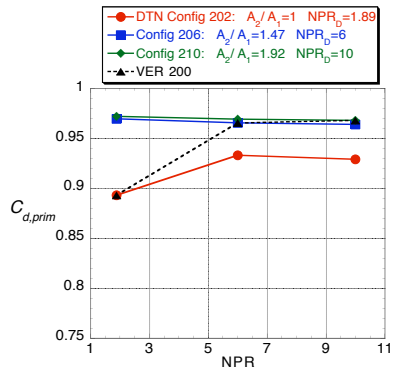

(a) l=5.26 in., l_1=4.04 in., l_2=1.22 in.

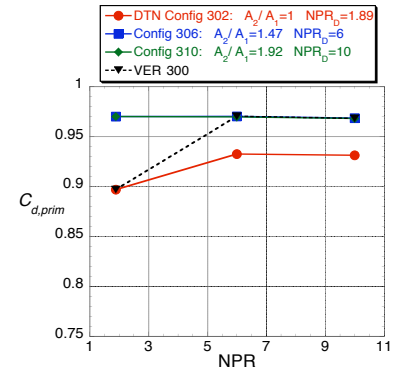

(b) l=4.21 in., l_1=3.225 in., l_2=0.985 in.

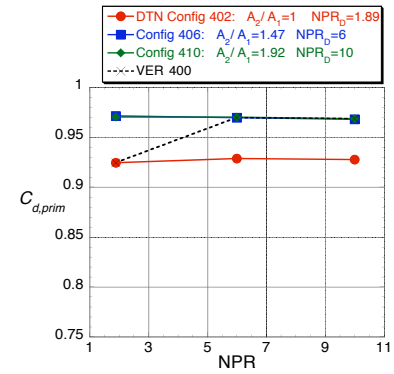

(c) l=4.21 in., l_1=2.836 in., l_2=1.374 in.

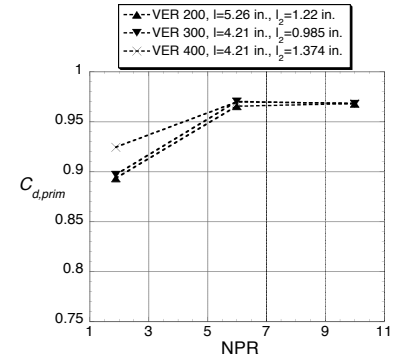

(d) Variable expansion ratio (VER) nozzles

Figure 16. Effect of a variable expansion ratio on unvectored (no injection) discharge coefficient.

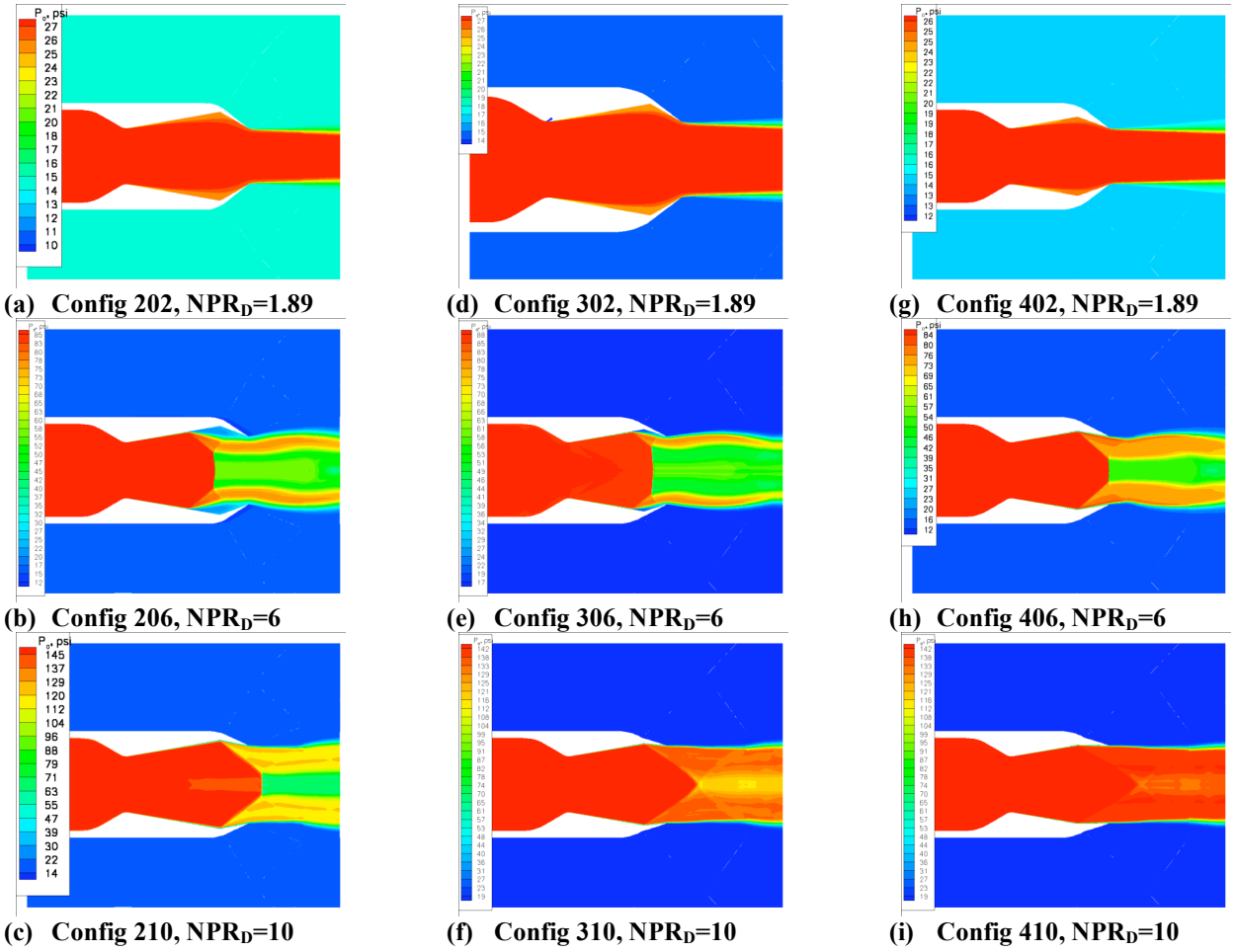

Figure 17. Total pressure contours at various expansion ratios and the design NPR, unvectored (no injection).

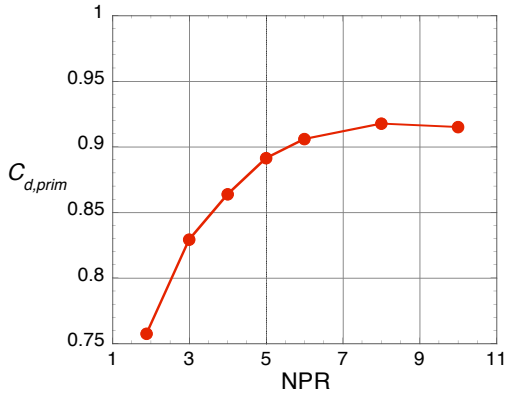

(a) Discharge coefficient

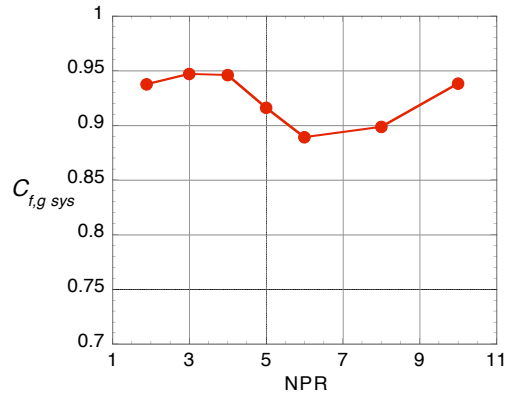

(b) System thrust ratio

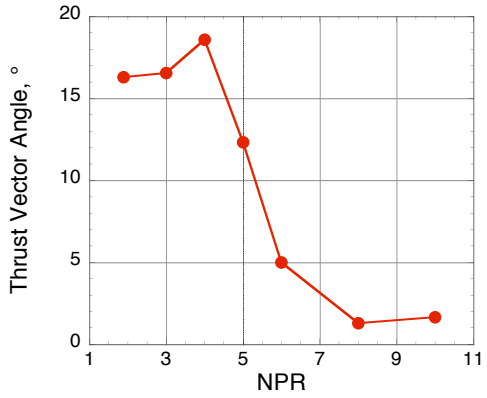

(c) Thrust vector angle

Figure 18. Effect of NPR on internal nozzle performance at variable expansion ratios (configurations 202-210, Table 3), 3% injection, M_∞=0.1.

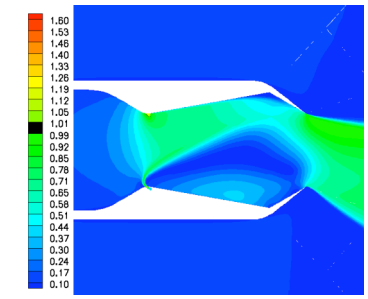

(a) NPR=1.89, A_2/A_1=1

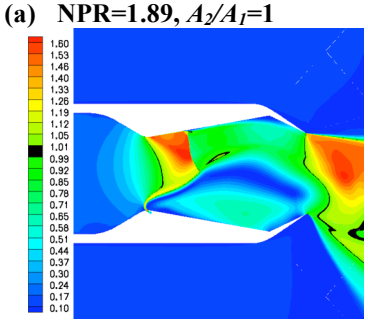

(b) NPR=4, A_2/A_1=1.22

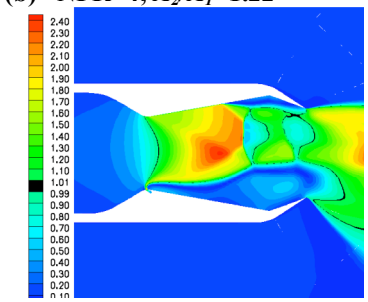

(c) NPR=6, A_2/A_1=1.47

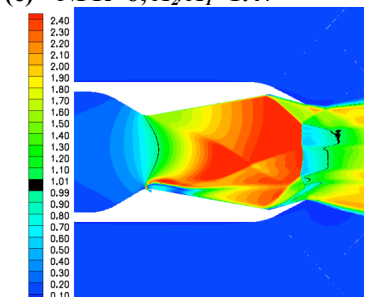

(d) NPR=8, A_2/A_1=1.7

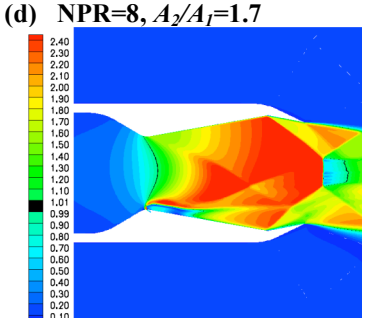

(e) NPR=10, A_2/A_1=1.92

Figure 19. Effect of NPR on Mach contours at variable expansion ratios (configurations 202-210, Table 3), 3% injection, M_∞=0.1.

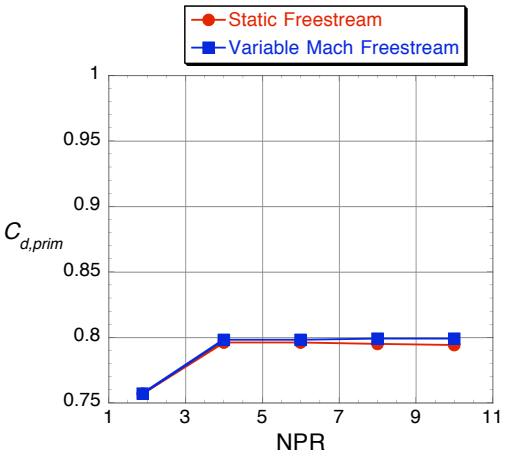

(a) Discharge coefficient

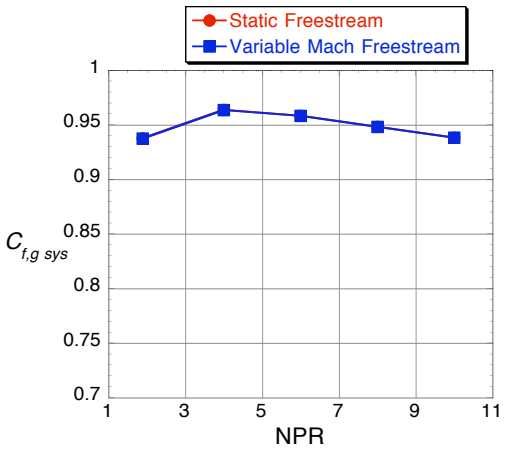

(b) System thrust ratio

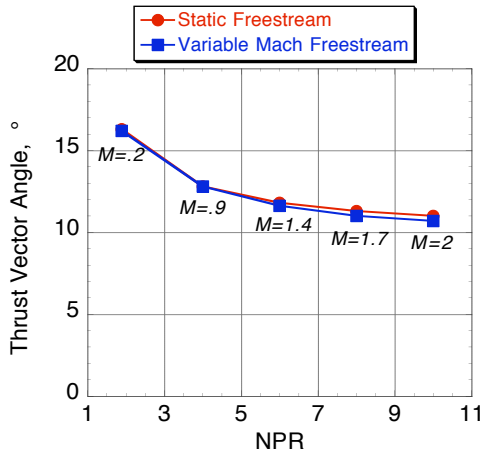

(c) Thrust vector angle

Figure 20. Effect of freestream flow on nozzle performance for the DTN (config 202, A_2/A_1=1) operating over a range of NPR and freestream Mach numbers with 3% fluidic injection.

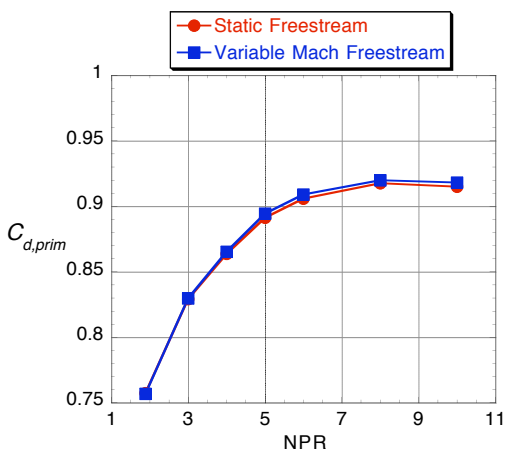

(a) Discharge coefficient

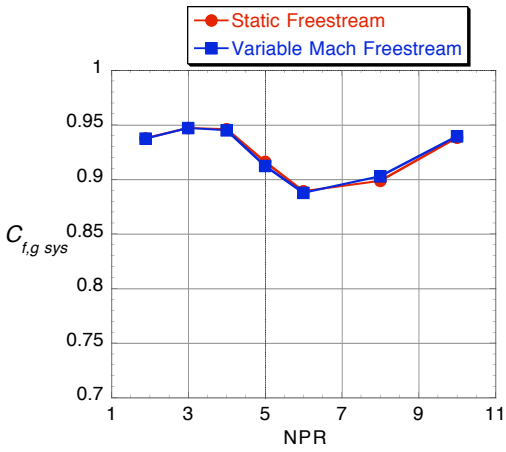

(b) System thrust ratio

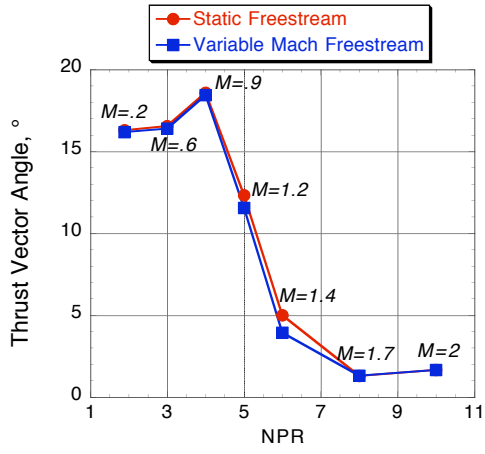

(c) Thrust vector angle

Figure 21. Effect of freestream flow on nozzle performance for the DTN with variable expansion ratios (configurations 202-210) operating over a range of NPR and freestream Mach numbers, 3% injection.

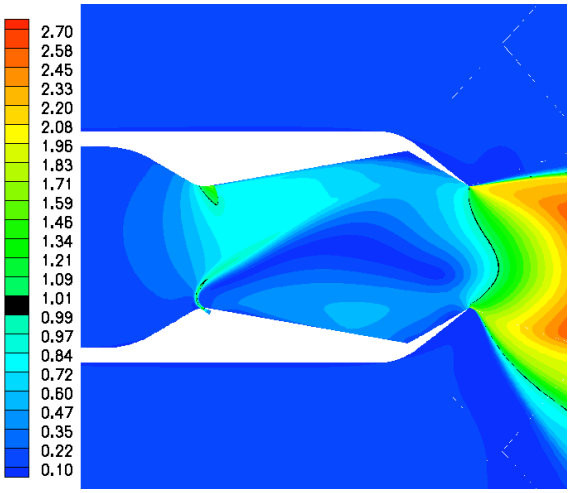

(a) M_∞=0.1

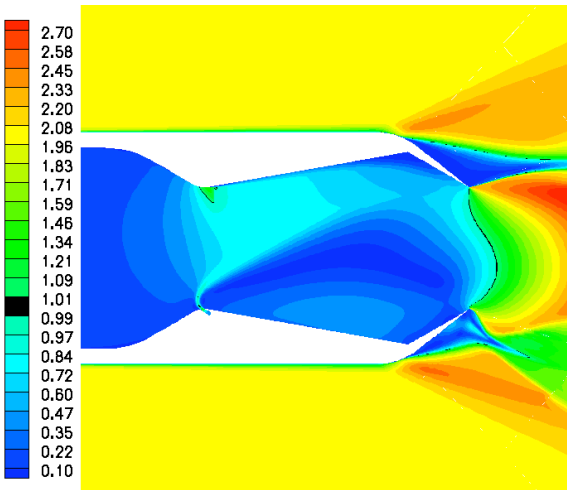

(b) M_∞=2

Figure 22. Effect of freestream flow on Mach contours for the DTN (config 202, A_2/A_1=1) at NPR=10 with 3% injection.

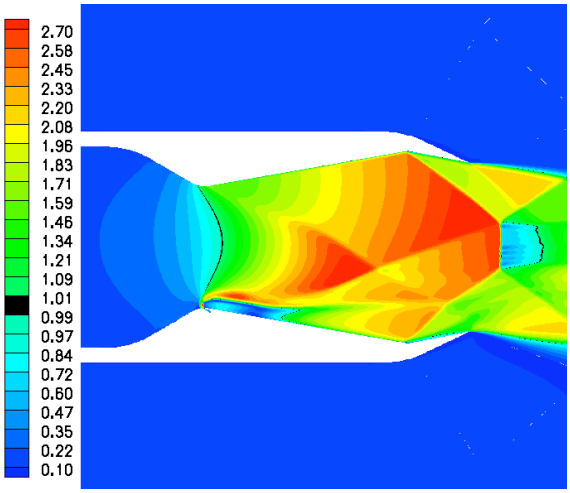

(a) M_∞=0.1

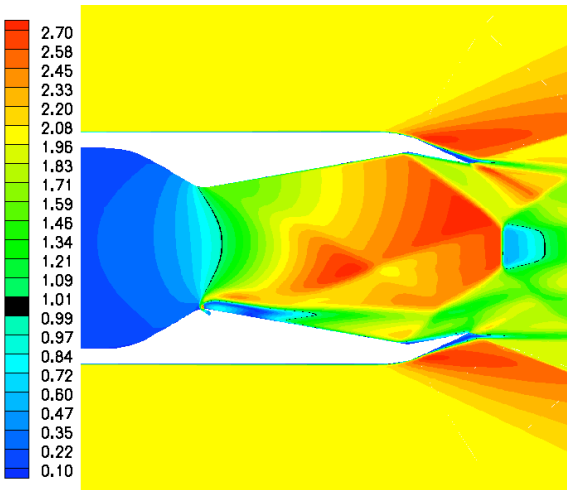

(b) M_∞=2

Figure 23. Effect of freestream flow on Mach contours for the expansion ratio A_2/A_1=1.92 nozzle at NPR=10 with 3% injection.